

Effects of infiltration parameters on mechanical and microstructural properties of tungsten wire reinforced $\text{Cu}_{47}\text{Ti}_{33}\text{Zr}_{11}\text{Ni}_6\text{Sn}_2\text{Si}_1$ metallic glass matrix composites

N. KHADEMIAN¹, R. GHOLAMIPOUR²

1. Department of Mechanics, Islamshahr Branch, Islamic Azad University, Tehran, Iran;
2. Iranian Research Organization for Science and Technology (IROST), Tehran, Iran

Received 30 May 2012; accepted 7 November 2012

Abstract: $\text{Cu}_{47}\text{Ti}_{33}\text{Zr}_{11}\text{Ni}_6\text{Sn}_2\text{Si}_1$ -based bulk metallic glass matrix composites reinforced with tungsten wires were fabricated by infiltration process at different temperatures (850, 900, 950 and 1000 °C) and time (10, 20 and 30 min) in a quartz or a steel tube. The mechanical tests were carried out by scanning electron microscopy (SEM) and X-ray diffraction (XRD). The results show that the maximum strength and total strain of the composite are 1778 MPa and 2.8% fabricated in steel tube at 900 °C for 10 min, and 1582 MPa and 3.6% fabricated in quartz tube at 850 °C for 10 min, respectively.

Key words: bulk metallic glass; metal matrix composite; tungsten wire; infiltration process; mechanical property; microstructure

1 Introduction

Bulk metallic glasses (BMGs) as potential candidate materials in various engineering fields, are characterized by high strength, high elastic strain limit and hardness [1]. Most monolithic metallic glasses tend to form localized shear band, resulting in limitation of plasticity under tension and compression and exhibiting catastrophic failure. Thus, the applications of bulk metallic glasses have been limited. On the other hand, many attempts have been adopted to enhance the toughness of metallic glasses such as introducing many in-situ and ex-situ composites systems [2]. The improvement of toughness and mechanical behavior in BMG matrix composites have been focused on different microstructural features and various processes [3–5].

It was reported that Zr–Ti–Ni–Cu–Be [6], Zr–Nb–Al–Cu–Ni [7], Zr–Ti–Al–Cu–Ni [8] and Zr–Al–Ni–Cu–Si [9] bulk metallic glasses were used as the matrices of the metal matrix composites; it was found that tungsten wire reinforcement increased compressive strain compared with unreinforced BMGs.

Compared with Zr-based bulk metallic glasses, Cu-based bulk metallic glasses have greater strength, lower price as well as higher density. Therefore, the

researchers have been attracted to identify processable Cu-based bulk metallic glasses with high toughness [10–13]. Recently, a $\text{Cu}_{47}\text{Ti}_{33}\text{Zr}_{11}\text{Ni}_6\text{Sn}_2\text{Si}_1$ alloy has been developed with a 6 mm-casting in critical diameter which is a relatively high GFA among Cu-based bulk metallic glasses [14].

In this study, a $\text{Cu}_{47}\text{Ti}_{33}\text{Zr}_{11}\text{Ni}_6\text{Sn}_2\text{Si}_1$ (mole fraction, %) BMG/ tungsten wires reinforced composite was produced and a detailed characterization of microstructure and mechanical properties of the composite was introduced.

2 Experimental

Alloy ingot with nominal composition of $\text{Cu}_{47}\text{Ti}_{33}\text{Zr}_{11}\text{Ni}_6\text{Sn}_2\text{Si}_1$ (mole fraction, %) was prepared by arc melting a mixture of pure metal elements in a titanium-gettered argon atmosphere, followed by melt suction casting into cylindrical water-cooled copper moulds. Tungsten wires with a nominal diameter of 800 μm were straightened and cut to 6 cm in length. These tungsten wires were degreased by ultrasonic cleaning in a acetone bath followed by the same procedure in a ethanol bath. Composite specimens were cast in an evacuated 304 stainless steel or a quartz tube (or mould) packed with the wires (60% in volume fraction) in a

resistive furnace by melting the ingots, and held at different temperatures (850, 900, 950 and 1000 °C) for different holding time of 10, 20 and 30 min, under 0.35 MPa of argon gas applied above the melt in order to ensure the infiltration of the molten alloys into the wires, followed by water quenching.

The microstructures of the samples were characterized on a scanning electron microscope (SEM) and an energy dispersive spectroscope (EDS). The phase analysis of the composites was carried out using X-ray diffraction (XRD) with the Cu K_{α} and Co K_{α} radiations. The deformation behavior and the mechanical properties under compression were done by an Instron testing machine at a strain rate of $1 \times 10^{-4} \text{ s}^{-1}$ at room temperature. The test samples with 5 mm in diameter and 10 mm in length were prepared by mechanically polishing in a regular fixture to ensure the parallelism of the ends. After mechanical tests, all the specimens were examined by SEM to reveal deformation and fracture features.

3 Results

3.1 Composites prepared in steel tubes

Figure 1 shows the X-ray diffraction patterns of the $\text{Cu}_{47}\text{Ti}_{33}\text{Zr}_{11}\text{Ni}_6\text{Sn}_2\text{Si}_1$ glassy alloy prepared in the steel tube. The unreinforced matrix pattern shows a broad diffraction peak, a typical profile of an amorphous structure. In the composites, the W diffraction peaks were superimposed on diffuse peak, but the intensity of amorphous peak is reduced for bulk metallic glass matrix composites related to the monolithic BMG structure. This indicates that the volume fraction of the amorphous phase in the matrix is reduced as a result of the formation of some crystalline phases. Cu_8Zr_3 , $\text{Cu}_{10}\text{Zr}_7$, CuTi_3 , Cu_4Ti_3 and Fe_2Ti phases can be indexed in the diffraction

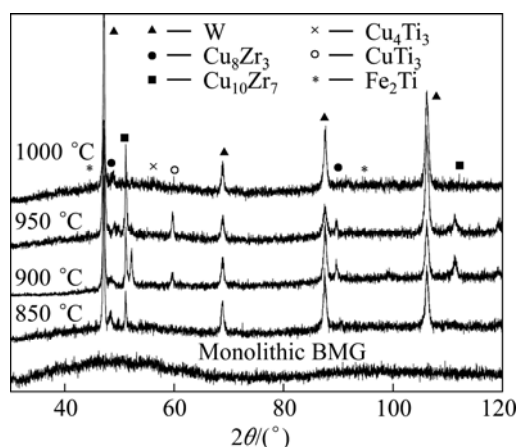


Fig. 1 XRD patterns of $\text{Cu}_{47}\text{Ti}_{33}\text{Zr}_{11}\text{Ni}_6\text{Sn}_2\text{Si}_1$ bulk metallic glass treated at different temperatures for 20 min

patterns of the composites. Iron source of Fe_2Ti phase is expected to originate from steel tube which reacted with the molten matrix during infiltration process.

During the preparation of composite in steel tube, different phases were formed as shown in Fig. 2. They are identified as polygonal phase, layered colony phase and dendrite-like phase. The increase of temperature or time of the process causes a change of phase morphology from layered colony phase to dendrite-like one, homogeneously dispersing in the matrix. EDS analysis indicates that the layered colony phase (<5 μm in diameter) is Cu- and Zr-rich phase and the polygonal phase is rich in Ti and Cu, as reported in Table 1. The XRD results shown in Fig. 1 also confirm the formation of the phases.

Figure 2(b) shows the SEM backscattered electron image of the dendrite-like phase at a high magnification. The dendrite-like structure can be characterized by primary dendrite arms with a length of 5–20 μm and the maximum volume fraction of 40%. EDS analysis reveals that the composition of the dendrite-like phase is rich in Zr, Cu and Ti (Table 2).

Table 1 EDS analyses of components of layered colony phase

Element	$w_{\text{unn}}/\%$	$w_{\text{norm}}/\%$	$x/\%$
Ti	6.04	6.51	9.22
Fe	1.33	1.43	1.73
Ni	1.86	2.01	2.32
Cu	57.64	62.10	66.27
Zr	24.17	26.04	19.36
Sn	1.78	1.92	1.09
Total	92.8		

Table 2 EDS analyses of components of dendrite like phase

Element	$w_{\text{unn}}/\%$	$w_{\text{norm}}/\%$	$x/\%$
Ti	19.06	22.08	28.48
Fe	5.65	6.55	7.24
Ni	3.36	4.20	4.42
Cu	38.25	44.30	43.05
Zr	16.01	18.54	12.55
Sn	2.75	3.19	1.66
Total	85.3		

Figure 2(d) shows the SEM micrograph of interfacial region of the composite between the matrix and steel tube. The increase of temperature enhances either the thickness of the reaction layer or the volume fraction of Fe-containing phase as a Fe_2Ti compound, which is agreement with XRD results shown in Fig. 1. A reaction layer with a skullcap shape and a thickness less than 6 μm was formed near the steel tube of the sample at 1000 °C for 30 min. The Fe-rich phase can be observed in the matrix at the maximum 50 μm away from the steel tube as seen in Fig. 2(d).

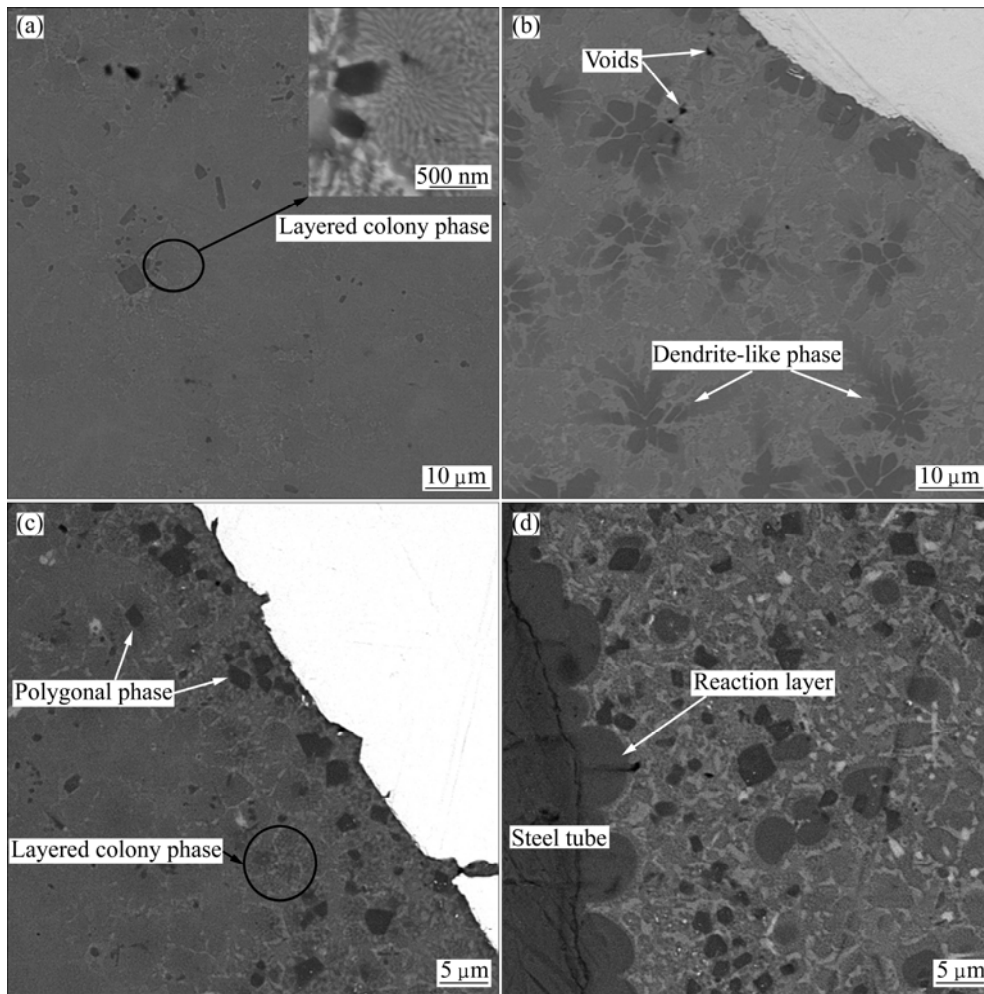


Fig. 2 SEM images of $\text{Cu}_{47}\text{Ti}_{33}\text{Zr}_{11}\text{Ni}_6\text{Sn}_2\text{Si}_1$ BMG matrix composites fabricated in steel tube at 850 °C for 20 min (a), at 900 °C for 10 min (b), and at 1000 °C for 30 min near tungsten wire (c) and in steel tube (d)

Figure 3 shows the quasistatic compressive stress—strain curves of the as-cast BMG and the composite samples prepared in the steel tube. The monolithic bulk metallic glass has 1% total deformation with ultimate strength of 1505 MPa; while in the sample fabricated at 900 °C for 10 min, the ultimate strength, strain at ultimate strength and strain at fracture are 1778 MPa, 2.6% and 2.8%, respectively. It can be found that the increase of infiltration temperature or time reduces the ultimate strength and total strain for composites. Figure 4 shows the specific absorbed energy or toughness (the area under the compressive stress—strain curves) of the samples prepared in steel tube. It is clear that the increase of infiltration temperature or time significantly reduces the toughness.

3.2 Composites prepared in quartz tubes

Figure 5 illustrates the XRD patterns of composite samples prepared in the quartz tube. As can be observed, Cu_8Zr_3 , $\text{Cu}_{10}\text{Zr}_7$, CuTi_2 , SnZr and Zr_5Sn_3 phases can be observed.

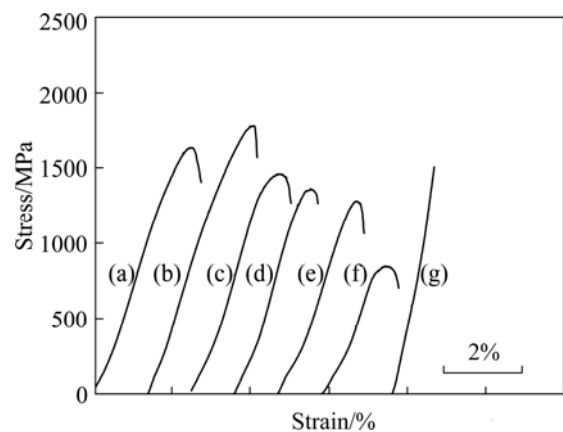


Fig. 3 Stress—strain curves for $\text{Cu}_{47}\text{Ti}_{33}\text{Zr}_{11}\text{Ni}_6\text{Sn}_2\text{Si}_1$ BMG matrix composites under quasi-static compression fabricated in steel tube at 850 °C for 20 min (a), 900 °C for 10 min (b), 900 °C for 20 min (c), 950 °C for 20 min (d), 1000 °C for 20 min (e), 1000 °C for 30 min (f) and monolithic BMG (g)

Figure 6 shows the SEM images of $\text{Cu}_{47}\text{Ti}_{33}\text{Zr}_{11}\text{Ni}_6\text{Sn}_2\text{Si}_1$ matrix composites prepared in the quartz tube at different temperatures and time. Figure 6(a)

indicates several phases as follows: martensite-like, needle-like, spherical-like and polygon phases with 55%, 3.5%, 3.5% and 1.5% in volume fraction, respectively. Based on the EDS results (not shown here), the martensite-like phase is Cu- and Zr-rich phase, the

needlelike and the spherical-like phases are Sn- and Zr-rich phase and the polygon phase is poor in Zr or rich in Ti and Cu. As can be seen in Fig. 6, the increase of temperature from 850 to 1000 °C causes the increase of volume fraction of the martensite-like phase from 55%

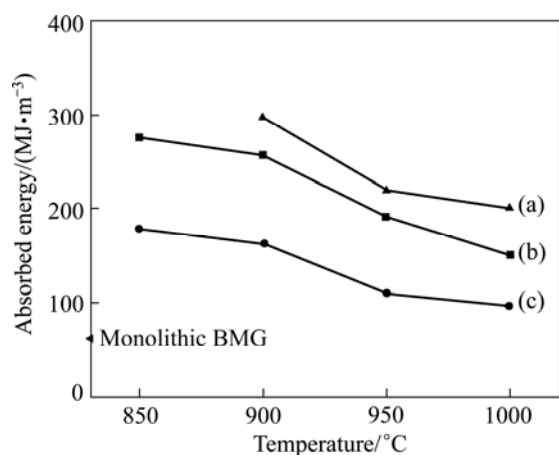


Fig. 4 Absorbed energy (toughness) versus temperature of composite fabricated in steel tube for 10 min (a), 20 min (b), 30 min (c) and monolithic BMG

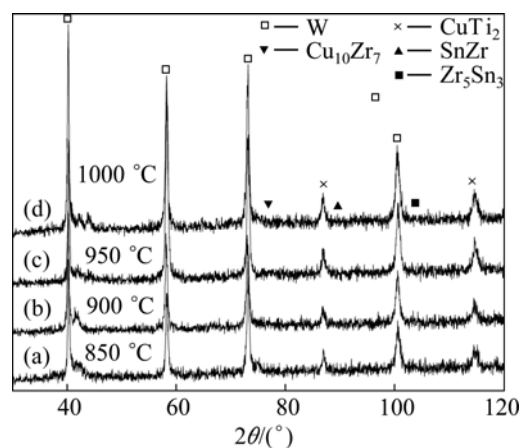


Fig. 5 XRD patterns of BMG matrix composites fabricated in quartz tube at 850 °C (a), 900 °C (b), 950 °C (c) and 1000 °C (d) for 20 min

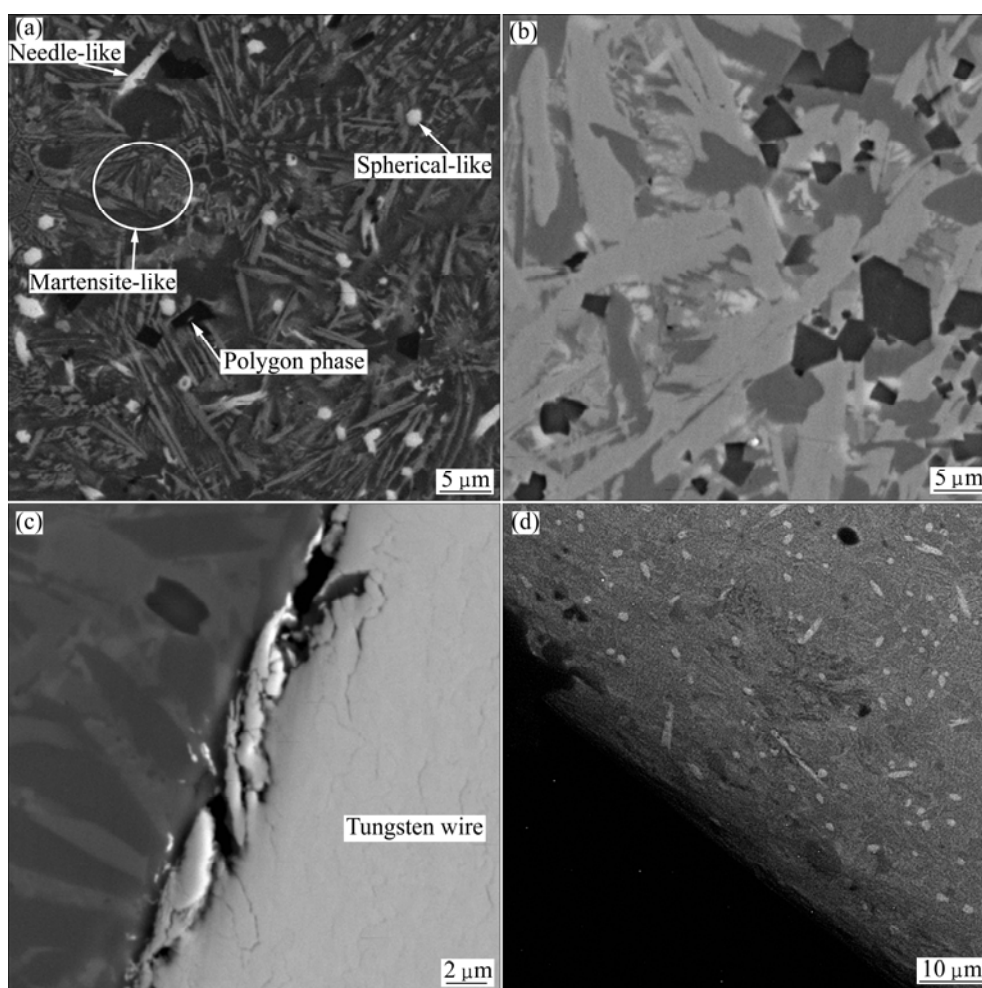


Fig. 6 SEM images of $\text{Cu}_{47}\text{Ti}_{33}\text{Zr}_{11}\text{Ni}_6\text{Sn}_2\text{Si}_1$ BMG matrix composites fabricated in quartz tube at 850 °C for 10 min (a), at 1000 °C for 30 min in matrix (b), at 1000 °C for 30 min in matrix near tungsten wire (c) and at 950 °C for 20 min near quartz tube (d)

to 60%, the morphology changes of needle-like and spherical-like phases to shapeless one with constant volume fraction (Fig. 6(b)), and finally, the increase of volume fraction of polygon phase from 1.5% to 10%.

There is not any significant interfacial reaction between the matrix and reinforcement as well as the matrix and quartz tube at the process temperature lower than 1000 °C, as can be observed from Figs. 6(a) to (c). However, some deterioration can be seen in tungsten wires in the microstructure of the sample prepared at the temperature of 1000 °C (Fig. 6(c)).

Figure 7 shows the quasistatic compressive stress—strain curves of the composite samples prepared in quartz tube at 850 °C for 10 min. It can be obtained the ultimate strength of 1582 MPa, strain at ultimate strength 2.4% and strain at fracture 3.6%. Figure 8 shows the specific absorbed energy or toughness of the samples prepared in

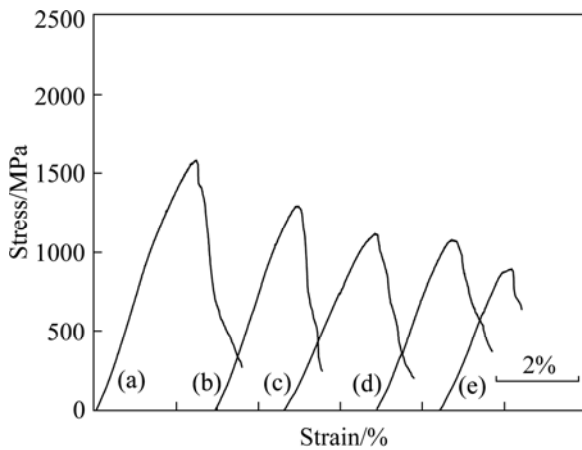


Fig. 7 Stress—strain curves of $\text{Cu}_{47}\text{Ti}_{33}\text{Zr}_{11}\text{Ni}_6\text{Sn}_2\text{Si}_1$ BMG matrix composites under quasi-static compression fabricated in quartz tube at 850 °C (a), 900 °C (b), 950 °C (c), 1000 °C (d) for 10 min and 1000 °C for 30 min (e)

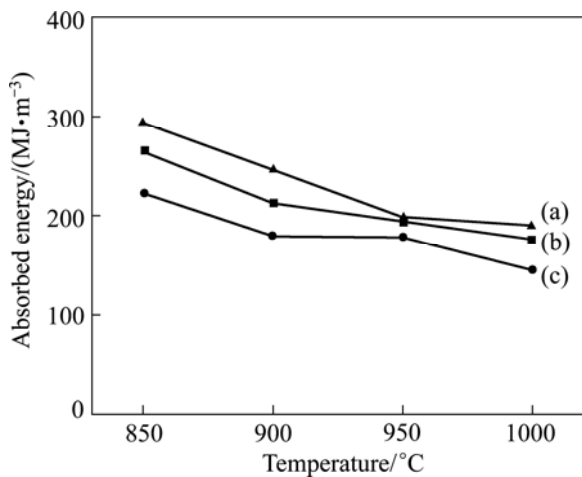


Fig. 8 Absorbed energy (toughness) of composite versus temperature fabricated in quartz tube for 10 min (a), 20 min (b) and 30 min (c)

quartz tube. It is clear that the increase of infiltration time and temperature significantly reduces the toughness of the samples.

Figure 9 shows the SEM secondary images of the fractography of the composites. Figure 9(a) shows the lateral surface of W_f /composite fabricated in the quartz tube at 950 °C for 10 min after compressing failure. It is

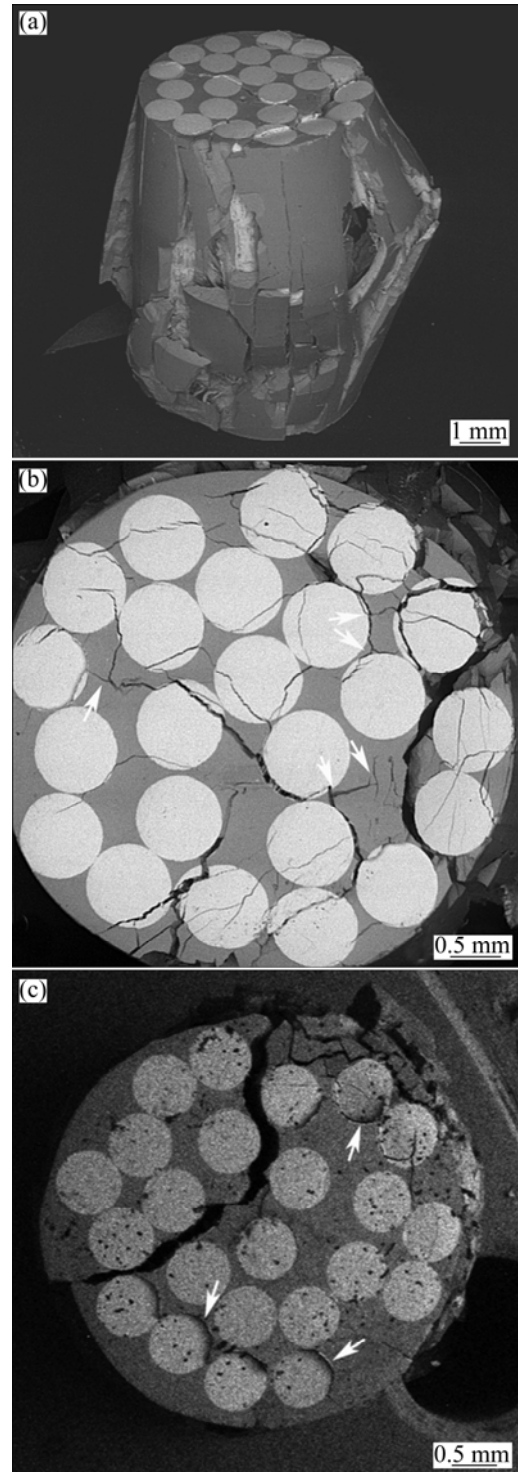


Fig. 9 SEM images of failed specimens prepared in quartz tube at 950 °C for 10 min (a), at 850 °C for 10 min (b) and at 1000 °C for 30 min (c)

observed the sample buckling and longitudinal splitting. Figure 9(b) shows the cross-section surface of the composite fabricated in the quartz tube at 850 °C for 10 min, while several cracks occur through the wire and matrix. Figure 9(c) shows the cross-section surface of the composite fabricated in the quartz tube at 1000 °C for 30 min, which reveals a single crack just through the matrix.

4 Discussion

Negative mixing enthalpies of Cu–Zr, Cu–Ti, Sn–Zr and Fe–Ti are –142, –78, –201 and –82 kJ/mol, respectively [15]. On the other hand, Cu, Zr, and Ti are all the main components of the matrix. Thus, based on the thermodynamical and kinetics aspects [16–20], it is expected that Cu–Zr and Cu–Ti compounds can be formed, as seen in Figs. 1, 2, 5 and 6. Although the thermodynamical condition of Sn–Zr compound formation is reasonable, the low level of Sn in chemical composition of the matrix makes it impossible for the Sn-rich phase to have kinetics conditions. Unless the cooling rate of solidification reaches a low level (in quartz tube), Sn atoms with a high atomic radius compared with other constituents (0.162 nm) can find enough time to diffuse during segregation process and react with other atoms. Finally, the finger print of the compound appears, as shown in Fig. 5.

In the steel tube, as a main source of Fe atoms, the conditions are perfectly ready for the solution of Fe atoms in the melt and substantially its reaction with the constituents of the matrix especially at high temperatures for a long time in infiltration process. Thus one can see Fe–Ti compounds (Fig. 2(d)). Moreover, a deterioration of the chemical composition of matrix from the optimum one to the highest glass forming ability [8] is another effect of the solution of Fe. On the other hand, although there is enough time to have any reaction between matrix and quartz, little evidence of the contamination of matrix from the tube can be observed in the samples prepared in the quartz tube (Fig. 6(d)). This phenomenon probably occurs due to the higher strength among Ionic SiO₂ (quartz) bonds as contrasted with metallic Fe bonds (steel).

It is well known that the heat conduction coefficient of steel is greater than that of quartz tube, thus the cooling rate during the solidification of matrix in the former is higher than that of the latter. This is the main reason of differences in morphology, size, distribution, type and volume fraction of phases presented in the matrices of the composites, though deterioration from highly GFA composition of matrix during infiltration is another major reason of phase selection in the final structure of the samples. Therefore, the type of the tube in infiltration of the BMGCs plays a major role in the

formation of different structures of the composites, particularly for the relatively high temperature or time of the process.

The mechanical characteristics of a wire-reinforced composite depend not only on the properties of the wire and the matrix, but also on the degree to which an applied load is transmitted to the wires by the matrix. The extent of this load transmittance is due to the magnitude of the interfacial bond between the fiber and matrix phases [21].

The difference between calculated and measured elastic moduli is an appropriate way to show mechanical behavior of the composite. Based on the mixture rule, elastic modulus E_C of a composite can be calculated by

$$E_C = E_f V_f + E_m V_m$$

where E_m and E_f , V_m and V_f are elastic moduli and volume fractions of a matrix (BMG) and fiber (tungsten wire), respectively. E_m and E_f are 110 and 410 GPa [22] and V_m and V_f are 40% and 60%, respectively. Thus, the elastic modulus of the composite can be calculated as 290 GPa. The measured elastic moduli of the samples fabricated at 900 °C for 10 min and at 1000 °C for 30 min in the steel tube are 270 and 191 GPa, respectively. This may be due to the weakness of interfacial bonds [5,23] or void formation [24] during the transformation of amorphous to crystalline phase (or phases) as shown in Fig. 2(b).

The increase of temperature and time of infiltration process may provide a condition for the formation of an appropriate interfacial bond [25]. On the other hand, the increase of the above mentioned parameters creates the opportunity for the formation of some crystalline phases in the matrices. Therefore, the increase of the parameters may give rise to two opposite conditions for the mechanical behavior of the composites: one is the improvement of interfacial bonding between the wires and matrices leading to the enhancement of mechanical properties of the samples as shown in Fig. 3 where the increase of the properties of the samples prepared in the steel tube is due to the increase of infiltration temperature from 850 to 900 °C. The second is the increase of the volume fraction of different crystalline phases as well as their morphologies resulting in the deterioration of mechanical properties of the samples prepared in the steel tube at 900 °C for 10 min. Thus the optimum conditions of the process in the steel tube are achieved by the infiltration at 900 °C for 10 min exhibiting the best mechanical properties. In the quartz tube, the improvement of the strength of the samples made at the medium selected temperatures of infiltration, i.e., the increase of temperature and time resulting in a continuous decrease of strength of the samples cannot be observed. This is due to the characteristics of the phases

with a sharp corner formed in matrices, leading to the disappearance of the interfacial bonds effect. The presence of these phases and thermal residual stresses started to build up from the glass transition temperature due to the fact that the different thermal expansion coefficients of the wires and matrices are all the sources of locally inhomogeneous strains. Based on the different analyses, the phases as well as residual stresses increase with increasing the temperature or time. Therefore, a low absorbed energy material in steel or quartz tube is gained, as shown in Figs. 4 and 8. Some researchers have already reported [26–29] that the conditions discussed above can occur during the cooling process and create some complex stresses such as axial, radial and hoop ones and finally induced longitudinal [21], transversal [30] and circumferential [31–33] cracks in the structure of infiltrated composites.

The mechanisms of toughening are defined as crack deflection [33], microcracking [34], blocking [27] and debonding [7]. Although one of these mechanisms is a dominant depending on the crystalline phases and interfacial properties, it may be the case that all mechanisms can be operative at the same time in a composite.

The driving force for deflection or crack deviation is the residual stress distribution [9,26] produced by the mismatch of thermal expansion between the fiber and matrix [30]. The crack deviation is an effective mechanism especially in zones with large space between wires, as shown in Fig. 9(b). Furthermore, this condition can be favorable to allow the stress field of the propagating micro crack to interact with the stress field around the reinforcement resulting in blunting, branching (see Fig. 9(b)), and a decrease of crack strain energy.

If fiber–matrix interfacial bond is weak, the fibers will debond [35] and then partially come out of the matrix as the cracks propagate through the composites prepared at a high temperature for long time in infiltration, as shown in Fig. 9(c). In this case, energy absorbing mechanism is friction between the fiber and the matrix. When the stress approached the ultimate strength, the failure was accompanied by buckling [32] of wires, as shown in Fig. 9(a).

5 Conclusions

1) The optimum infiltration temperature and time were found to be 900 °C and 10 min for sample fabricated in the steel tube and 850 °C and 10 min for sample fabricated in the quartz tube.

2) The ultimate strength, the strain at ultimate strength and the strain at fracture of 1778 MPa, 2.6% and 2.8%, respectively are the best mechanical properties for sample fabricated at optimum conditions in steel tube.

References

- [1] QIAO J W, ZHANG Y, CHEN G L. Fabrication and mechanical characterization of a series of plastic Zr-based bulk metallic glass matrix composites [J]. *Materials and Design*, 2009, 30: 3966–3971.
- [2] WANG W H. Roles of minor additions in formation and properties of bulk metallic glasses [J]. *Progress Mater Science*, 2007, 52: 540–596.
- [3] ZHANG Y, ZHOU Y, HUI X, WANG M, CHEN G. Minor alloying behavior in bulk metallic glasses and high-entropy alloys [J]. *Science in China Series G*, 2008, 51(4): 427–437.
- [4] WANG S, ZHANG Y. Shear-band spacing controlled by Bridgman solidification in dendrite/BMG composites [J]. *Science in China Series G*, 2009, 52(10): 1632–1636.
- [5] QIU K Q, REN Y L. Melt infiltration casting of $Zr_{57}Al_{10}Nb_5Cu_{15.4}Ni_{12.6}$ amorphous matrix composite [J]. *J Miner Mater Character Eng*, 2004, 3: 91–98.
- [6] DANDLIKER R B, CONNER R D, JOHNSON W L. Melt infiltration casting of bulk metallic-glass matrix composites [J]. *J Mater Res*, 1998, 13: 2896–2901.
- [7] YIM H C, CONNER R D, SZUECS F, JOHNSON W L. Processing, microstructure and properties of ductile metal particulate reinforced $Zr_{57}Nb_5Al_{10}Cu_{15.4}Ni_{12.6}$ bulk metallic glass composites [J]. *Acta Mater*, 2002, 50: 2737–2745.
- [8] YIM H C, JOHNSON W L. Bulk metallic glass matrix composites [J]. *Appl Phys Lett*, 1997, 71: 3808–3810.
- [9] QIU K Q, WANG A M, ZHANG H F, DING B Z, HU Z Q. Mechanical properties of tungsten fiber reinforced ZrAlNiCuSi metallic glass matrix composite [J]. *Intermetallics*, 2002, 10: 1283–1288.
- [10] INOUE A, ZHANG W, ZHANG T, KUROSAKA K. Cu-based bulk glassy alloys with high tensile strength of over 2000 MPa [J]. *J Non-Cryst Solids*, 2002, 304: 200–209.
- [11] ECKERT J, DAS J, KIM KB, BAIER F, TANG M B, WANG W H, ZHANG Z F. High strength ductile Cu-base metallic glass [J]. *Intermetallics*, 2006, 14: 876–881.
- [12] ZHANG Q, ZHANG W, INOUE A. New Cu–Zr-based bulk metallic glasses with large diameters of up to 1.5 cm [J]. *Scripta Mater*, 2006, 55: 711–713.
- [13] DAS J, TANG M, KIM K B, THEISSMANN R, BAIER F, WANG W H, ECKERT J. Work-hardenable ductile bulk metallic glass [J]. *Physical Review Letters*, 2005, 94: 205501.
- [14] PARK E S, LIM H K, KIM W T, KIM D H. The effect of Sn addition on the glass forming ability of Cu–Ti–Zr–Ni–Si metallic glass alloys [J]. *J Non-Cryst Solids*, 2002, 298: 15–22.
- [15] MIEDMA A R, BOER F R D, BOOM R. Model predictions for the enthalpy of formation of transition metal alloys [J]. *CALPHAD*, 1977, 1(4): 341–359.
- [16] LOFFLER J F. Bulk metallic glasses [J]. *Intermetallics*, 2003; 11: 529–540.
- [17] HADEK M A E, KASSEM M. Failure behavior of Cu–Ti–Zr-based bulk metallic glass alloys [J]. *J Mater Sci*, 2009, 44: 1127–1136.
- [18] BAE D H, LIM H K, KIM S H, KIM D H, KIM W T. Mechanical behaviour of a bulk Cu–Ti–Zr–Ni–Si–Sn metallic glass forming nano-crystal aggregate bands during deformation in the supercooled liquid region [J]. *Acta Mater*, 2002, 50: 1749–1752.
- [19] DAI C L, DENG J W, ZHANG Z X, XU J. Cu–Zr–Ti ternary bulk metallic glasses correlated with $(L_{Cu_8Zr_3+Cu_{10}Zr_7})$ univariant eutectic reaction [J]. *J Mater Res*, 2008, 23: 1249–1257.
- [20] KASAI M, MATSUBARA E, SAIDA J, NAKAYAMA M, UEMATSU K, ZHANG T, INOUE A. Crystallization behavior of $Cu_{60}Zr_{30}Ti_{10}$ bulk glassy alloy [J]. *Mater Sci Eng A*, 2004, 375–377:

- 744–748.
- [21] QIU K Q, SUE Z Y, REN Y L, YU B. Observation of shear bands formation on tungsten fiber-reinforced Zr-based bulk metallic glass matrix composite [J]. *J Mater Res*, 2007, 22: 551–554.
- [22] WANG G, CHEN D M, SHEN J, STACHURSKI Z H, QIN Q H, SUN J F, ZHOU B D. Deformation behaviours of a tungsten-wire/bulk metallic glass matrix composite in a wide strain rate range [J]. *J Non-Cryst Solids*, 2006, 352: 3872–3878.
- [23] WANG M L, CHEN G L, HUI X, ZHANG Y, BAI Z Y. Optimized interface and mechanical properties of W fiber/Zr-based bulk metallic glass composites by minor Nb addition [J]. *Intermetallics*, 2007, 15: 1309–1315.
- [24] ECKERT J, DAS J, LOSER W, ROY S K, GEBERT A. Strengthening of multicomponent glass-forming alloys by microstructure design [J]. *J Non-Cryst Solids*, 2007, 353: 3742–3749.
- [25] LIU N, MA G F, ZHANG H F, LI H, DING B Z, WANG A M, HU Z Q. Wetting behavior of Zr-based bulk metallic glasses on W substrate [J]. *Mater Letters*, 2008, 62: 3195–3197.
- [26] AYDINER C C, USTUNDAG E, CLAUSEN B, HANAN J C, WINHOLTZ R A, BOURKE M A M, PEKER A. Residual stresses in a bulk metallic glass-stainless steel composite [J]. *Mater Sci Eng A*, 2005, 399: 107–113.
- [27] LEE S Y, CLAUSEN B, USTUNDAG E, YIM H C, AYDINER C C, BOURKE M A M. Compressive behavior of wire reinforced bulk metallic glass matrix composites [J]. *Mater Sci Eng A*, 2005, 399: 128–133.
- [28] DRAGOI D, USTUNAG E, CLAUSEN B, BOURKE M A M. Investigation of thermal residual stresses in tungsten-fiber/bulk metallic glass matrix composites [J]. *Scripta Mater*, 2001, 45: 245–252.
- [29] CLAUSEN B, LEE S Y, USTUNDAG E, AYDINER C C, CONNER R D, BOURKE M A M. Compressive yielding of tungsten fiber reinforced bulk metallic glass composites [J]. *Scripta Mater*, 2003, 49: 123–128.
- [30] YIM H C, LEE S Y, CONNER R D. Mechanical behavior of Mo and Ta wire reinforced bulk metallic glass composites [J]. *Scripta Mater*, 2008, 58: 763–766.
- [31] LI H, SUBHASH G, KECSKES L J, DOWDING R J. Mechanical behavior of tungsten perform reinforced bulk metallic glass composites [J]. *Mater Sci Eng A*, 2005, 403: 134–143.
- [32] YIM H C, CONNER R D, SZUECS F, JOHNSON W L. Quasistatic and dynamic deformation of tungsten reinforced Zr₅₇Nb₅Al₁₀Cu_{15.4}Ni_{12.6} bulk metallic glass matrix composites [J]. *Scripta Mater*, 2001, 45: 1039–1045.
- [33] LIM H K, PARK E S, PARK J S, KIM W T, KIM D H. Fabrication and mechanical properties of WC particulate reinforced Cu₄₇Ti₃₃Zr₁₁Ni₆Sn₂Si₁ bulk metallic glass matrix composites [J]. *J Mater Sci*, 2005, 40: 6127–6130.
- [34] HUTCHINSON J W. Mechanisms of toughening in ceramics [J]. *Theoretical and Applied Mechanics*, 1989: 139–144.
- [35] QIU K Q, HAO D Z, REN Y L, ZHANG H. Mechanical properties for bulk metallic glass with crystallites precipitation and second ductile phase addition [J]. *J Mater Sci*, 2007, 42: 3223–3229.

渗透参数对钨丝增强 Cu₄₇Ti₃₃Zr₁₁Ni₆Sn₂Si₁ 金属玻璃基复合材料力学性能和显微组织的影响

N. KHADEMIAN¹, R. GHOLAMIPOUR²

1. Department of Mechanics, Islamshahr Branch, Islamic Azad University, Tehran, Iran;

2. Iranian Research Organization for Science and Technology (IROST), Tehran, Iran

摘要: 在不同温度(850, 900, 950 和 1000 °C)和时间(10, 20 和 30 min)下, 采用渗透工艺, 在石英管或钢管中制备钨丝增强 Cu₄₇Ti₃₃Zr₁₁Ni₆Sn₂Si₁ 金属玻璃基复合材料。利用扫描电子显微镜(SEM)和 X 射线衍射(XRD)技术研究样品的组织, 并测试了样品的力学性能。结果表明, 900 °C 时在钢管中渗透 10 min 制备的复合材料的最高强度和伸长率分别达到 1778 MPa 和 2.8%, 850 °C 时在石英管中渗透 10 min 制备的复合材料的最高强度和伸长率分别达到 1582 MPa 和 3.6%。

关键词: 块体金属玻璃; 金属基复合材料; 钨丝; 渗透工艺; 力学性能; 微观组织

(Edited by Xiang-qun LI)